Disorder and Nonstoichiometry in Synthetic Garnets $A_3B_5O_{12}$ (A = Y, Lu−La, B = Al, Fe, Ga). A Simulation Study

Chiara Milanese,[†] Vincenzo Buscaglia,*[,‡] Filippo Maglia,[†] and Umberto Anselmi-Tamburini[†]

Department of Physical Chemistry and IENI/CNR, University of Pavia, v.le Taramelli, 16, I-27100 Pavia, Italy, and Institute for Energetics and Interphases (IENI), National Research Council, Via De Marini 6, I-16149 Genova, Italy

Received October 8, 2003. Revised Manuscript Received January 13, 2004

Atomistic simulation calculations have been used to study disorder and deviation from stoichiometry in synthetic garnets $A_3B_5O_{12}$ as a function of A^{3+} (Y^{3+}, Lu^{3+} to La^{3+}) and B^{3+} (Al^{3+}, Ga^{3+}, Fe^{3+}) ionic radius. Trends corresponding to the energy of several defect reactions have been obtained. Results compare favorably with the available, albeit limited, experimental data. Disorder in garnets is dominated by formation of antisite defects and the corresponding energy decreases with decreasing A cation size. Incorporation of excess Y_2O_3 or rare-earth oxide is energetically preferred with respect to incorporation of excess B_2O_3 (B = Al, Fe, Ga). Solution of excess binary oxide occurs by the formation of antisites rather than vacancies. Neither an excess of A_2O_3 or B_2O_3 seems to be the main source of oxygen nonstoichiometry in Al and Ga garnets. On the contrary, accommodation of oxygen nonstoichiometry in iron garnets is energetically more favored if accompanied by the reduction of Fe(III) to Fe(II). The energy of formation of oxygen vacancies is lower for Lu, Yb, and Er iron garnets. Interactions between divalent iron and oxygen vacancies are discussed. Within the limitations of the present approach, the calculated trends contribute to the understanding of defect chemistry of garnets and provide suggestions for future experimental studies.

I. Introduction

Natural garnets form a widespread group of silicates occurring in many types of rocks. Synthetic garnets are oxide materials with several applications in technology. Yttrium aluminum garnet ($Y_3Al_5O_{12}$, YAG) and other garnets ($Y_3Ga_5O_{12}$, $Gd_3Ga_5O_{12}$, etc.) are well-known hosts for rare-earth and transition-metal ions in lasers and phosphors.[1] In addition, YAG is one of the most creep-resistant materials at high temperatures.[2−3] Yttrium iron garnet ($Y_3Fe_5O_{12}$, YIG) and rare-earth iron garnets are magnetic oxides with application in microwave and magnetooptic devices.[1,4] Nickel-doped and cerium-doped YAG, as well as YAG−YIG solid solutions, are mixed ionic−electronic conductors at high temperature.[5−7] Very recently, oxygen ionic conduction has been reported for $Y_3Fe_5O_{12}$ and $Gd_3Fe_5O_{12}$.[8] Thus, garnets also can be potential materials for high-temperature electrochemical applications, including solid oxide fuel cells. The physical processes at the root of the above properties are strongly related to the presence of lattice defects (either intrinsic or induced by incorporation of foreign atoms) and to nonstoichiometry. Only the defect structures of YIG and YAG have been investigated,[5−7,9−10] while scant information is available on the rare-earth garnets. However, a better knowledge of the defect structure of garnets would be desirable to tune their properties and even predict new applications.

The general chemical formula of an oxide garnet can be written as $A_3B_2C_3O_{12}$, with eight formula units (160 atoms) per unit cell. The space group is *Ia*3*d* with cubic symmetry. The trivalent cations are all in special positions with no positional degrees of freedom. The A ions occupy 24(c) dodecahedral sites. The B ions are at 16(a) octahedral sites, and the C ions fill the 24(d) tetrahedral sites. Here we have considered ternary synthetic garnets where B = C, like $Y_3Al_5O_{12}$, rather

* Corresponding author. Tel: +39-010-6475708. Fax: +39-010-6475700. E-mail: buscaglia@ge.ieni.cnr.it.

[†] Department of Physical Chemistry and IENI/CNR, University of Pavia.

[‡] Institute for Energetics and Interphases (IENI), National Research Council.

(1) Weber, M. J. The Role of Lanthanides in Optical Materials. In *Ceramic Transactions*; Potter, B. G., Jr., Bruce, A. J., Eds.; The American Ceramic Society: Westerville, OH, 1996; vol 67, pp 3−20.

(2) Parthasarathy, T. A.; Mah, T.-I.; Keller, K. *J. Am. Ceram. Soc.* **1992**, *75*, 1756.

(3) Corman, G. S. *J. Mater. Sci. Lett.* **1993**, *12*, 379.

(4) Gilleo, M. A. Ferromagnetic Insulators: Garnets. In *Ferro-Magnetic Materials*; Wohlfarth, E. P., Ed.; North-Holland: Amsterdam, The Netherlands, 1986; vol 2, pp 1−53.

(5) Rotman, S. R.; Tandon, R. P.; Tuller, H. L. *J. Appl. Phys.* **1985**, *57*, 1951.

(6) Rotman, S. R.; Tuller, H. L. *J. Appl. Phys.* **1987**, *62*, 1305.

(7) Rotman, S. R.; Tuller, H. L. *J. Electroceram.* **1998**, *2*, 95.

(8) Kharton, V. V.; Shaula, A. L.; Naumovich, E. N.; Vyshatko, N. P.; Marozau, I. P.; Viskup, A. P.; Marques, F. M. B. *J. Electrochem. Soc.* **2003**, *150*, J33.

(9) Metselaar, R.; Huyberts, M. A. H. *J. Phys. Chem. Solids* **1973**, *34*, 2257.

(10) Metselaar, R.; Huyberts, M. A. H. *J. Solid State Chem.* **1977**, *22*, 309.

10.1021/cm031138u CCC: $27.50
Published on Web 03/04/2004

than natural silicate garnets. The A ion can be Y^{3+} or a trivalent rare-earth ion of the lanthanide series (Ln^{3+}). The oxygen ions are all in the general position 96(h). Unit cell edge and oxygen position of many garnets can be found in Volume 12 of the Landolt-Börnstein series [11] or in the ICSD crystallographic database.[12]

Static-lattice techniques developed in the past 20 years and based on the concept of interatomic potential are nowadays widely recognized as a very useful tool to study defect formation in solids. The usefulness and the reliability of these techniques has been assessed for a large variety of oxides, including binary oxides, perovskites, high-T_c superconductors, pyrochlores, and zeolites.[13−20] Previous modeling studies of garnets have focused only on $Y_3Fe_5O_{12}$[21] and on $Y_3Al_5O_{12}$.[22,23] Those studies attempted to find the energetically most-favored defect processes among a variety of defect reactions. The simulations pointed out the importance of antisite defects in the development of disorder and nonstoichiometry in yttrium garnets.

The present study was aimed to get a better understanding of the trends involved in cation disorder and in nonstoichiometry of garnets with general formula $A_3B_5O_{12}$ as a function of A^{3+} (Y^{3+}, Lu^{3+} to La^{3+}) and B^{3+} (Al^{3+}, Ga^{3+}, Fe^{3+}) ionic radius.

II. Methodology and Interatomic Potentials

The atomic scale simulation techniques used here for both the perfect and the defective lattice are based on energy minimization. The general theory was reviewed by Catlow and Mackrodt.[24] The positions of the constituting species (ions) are systematically adjusted until the minimum energy configuration is found. At each step, the energy of the system is obtained by summing over the various interactions using specified interatomic potentials. For predominantly ionic systems, the pairwise potential

$$E_{ij} = \frac{1}{4\pi\epsilon_0}\frac{Z_i Z_j e^2}{r_{ij}} + A_{ij}\exp\left(-\frac{r_{ij}}{\rho_{ij}}\right) - \frac{C_{ij}}{r_{ij}^6} \qquad (1)$$

is generally used. The potential includes the long-range Coulombic term, the short-range repulsive force, and the short-range van der Waals force; r_{ij} is the distance between a given pair of ions, Z_i and Z_j are the formal valences, e is the electron charge, and A_{ij}, ρ_{ij}, and C_{ij} are the adjustable parameters. There is increasing evidence from ab initio electronic structure calculations that the trivalent ions included in this study have an effective charge (as derived by Mulliken population analysis or similar approaches) close to the formal charge Z. Ching and Xu[25] have obtained the following effective charges in yttrium aluminum garnet: 2.72 for Al, 2.50 for Y, and −1.76 for O. This result confirms the strong ionic character of $Y_3Al_5O_{12}$. The ionic character of $Gd_3Ga_5O_{12}$ is comparable to that of $Y_3Al_5O_{12}$.[26]

The electronic polarizability of ions is accounted for by the shell model of Dick and Overhauser.[27] Each ion is described in terms of a massive core of charge $X|e|$ connected by a harmonic spring with *force* constant k to a massless shell of charge $Y|e|$ on which all short-range pair potentials act. The formal charge of the ion corresponds to $Z = X + Y$ and its polarizability results

$$\alpha_i = \frac{Y_i^2 e^2}{k_i} \qquad (2)$$

The adjustable parameters in eq 1 and the shell parameters of the ions, Y and k, were determined by least-squares fitting of calculated to experimentally observable properties, including crystal structure (unit cell edge and oxygen position), elastic constants, static dielectric constant, and high-frequency dielectric constant. The potential parameters were obtained by simultaneous fitting of several garnets using the relaxed fitting strategy.[28] The multistructural fitting approach results in potentials reflecting the ion−ion interactions over a wide range of interatomic separations. This parametrization strategy generally produces more reliable potentials in comparison to the fit to a single structure. In the latter case, the parameters are strictly valid for interatomic distances corresponding to the equilibrium separation. In contrast, for defect calculations involving substantial lattice relaxation, the interatomic separations around lattice defects can be very different from those in the perfect crystal. Therefore, the quality of adopted potentials is of paramount importance. The fitting strategies and the related implications were discussed by Gale.[28] Once the parameters for the Al−O, Fe−O, and Ga−O interactions were obtained, they were used to determine the potentials corresponding to Ln−O interactions for some hypothetical garnets, like La garnets.

The defect energies were computed using a two-region strategy.[24] The first region (I) includes a spherical portion of the crystal surrounding the defect, while the second region (II) includes the remainder of the crystal. Interactions in region I are treated explicitly, and relaxation of the lattice under the action of the force field of the defect is allowed. In contrast to this atomistic treatment, the response of region II is evaluated using a more approximate approach, with the defect forces

(11) Hellwege, K.-H., Hellwege, A. M., Eds. *Landolt-Börnstein. Numerical Data and Functional Relationships in Science and Technology, Vol. 12a, Magnetic and Other Properties of Oxides and Related Compounds, Part a, Garnets and Perovskites*; Springer: Berlin, Germany, 1978.
(12) ICSD Inorganic Crystal Structure Database, Fachinformationszentrum, Karlsruhe, Germany, 2003.
(13) Tomlinson, S. M.; Catlow, C. R. A.; Harding, J. H. *J. Phys. Chem. Solids* **1990**, *51*, 477.
(14) Catlow, C. R. A.; Bell, R. G.; Gale, J. D. *J. Mater. Chem.* **1994**, *4*, 781.
(15) Islam, M. S.; Winch, L. J. *Phys. Rev. B* **1995**, 52, 10510.
(16) Islam, M. S. *J. Mater. Chem.* **2000**, *10*, 1027.
(17) Minervini, L.; Grimes, R. W.; Sickafus, K. E. *J. Am. Ceram. Soc.* **2000**, *83*, 1873.
(18) Stanek, C. R.; Minervini, L.; Grimes, R. W. *J. Am. Ceram. Soc.* **2002**, 85, 2792.
(19) Saadoune, I.; Catlow, C. R. A.; Cora, F. *Microporous Mesoporous Mater.* **2003**, *59*, 161.
(20) Sastre, G.; Gale, J. D. *Chem. Mater.* **2003**, *15*, 1788.
(21) Donnerberg, H.; Catlow, C. R. A. *J. Phys.: Condens. Matter* **1993**, 5, 2947.
(22) Kuklja, M. M.; Pandey, R. *J. Am. Ceram. Soc.* **1999**, *82*, 2881.
(23) Kuklja, M. M. *J. Phys.: Condens. Matter* **2000**, *12*, 2953.
(24) Catlow, C. R. A.; Mackrodt, W. C. *Lect. Notes Phys.* **1982**, *166*, 3.
(25) Ching, W. Y.; Xu, Y.-N. *Phys. Rev. B* **1999**, 59, 12815.
(26) Xu, Y.-N.; Ching, W. Y.; Brickeen, B. K. *Phys. Rev. B* **2000**, *61*, 1817.
(27) Dick, B. G.; Overhauser, A. W. *Phys. Rev.* **1958**, *112*, 90.
(28) Gale, J. D. *Philos. Mag. B* **1996**, *73*, 3.

being relatively weak owing to the increased distance between the defect and the atoms.[24] Smooth transition between regions I and II is accomplished by introducing an intermediate region, IIa, where interactions are treated by less expensive computational techniques than in region I. In the present calculations, the radii of regions I and IIa were 12.5 and 25 Å, respectively. Use of larger regions produces no significant changes on the defect formation energy. In all cases, calculations were conducted using the GULP code.[29] For each compound, the perfect lattice energy and individual defect energies have been obtained. In total, 240 separate calculations were performed for the isolated defects alone.

The type of calculations described here are called "static", because entropy and energy contributions from lattice vibrations are not included. Furthermore, configurational entropy is also neglected. However, some thermal effects are subsumed within the interatomic potentials, because the potential parameters were derived from the crystal structure and the lattice properties determined at room temperature. The inclusion of thermal effects in defect calculation will prohibitively increase the calculation time. The influence of temperature was explicitly considered only to predict the thermal expansion coefficient (TEC) of the perfect lattice. The calculation of the TEC was performed by minimization of the Gibbs free energy within the quasi-harmonic approximation. Integration across the Brillouin zone was carried out using the standard Monkhorst-Pack scheme for the generation of the integration grid. Convergence was checked by using different values of the grid spacing.

III. Results and Discussion

(1) Interatomic Potentials. The potential parameters derived according to the methodology described in Section II are reported in Table 1. Short-range repulsive interactions were considered only for oxygen−cation and oxygen−oxygen pairs, owing to the shorter interatomic separation in comparison to cation−cation distances. In YIG, for example, the interatomic distances (in Å) are as follows: 1.87 for Fe^{3+}(d)−O^{2-}, 2.01 for Fe^{3+}(a)−O^{2-}, 2.37 for Y^{3+}−O^{2-}, 2.68 for O^{2-}−O^{2-}, 3.09 for Y^{3+}−Fe^{3+}(d), 3.46 for Y^{3+}−Fe^{3+}(a), etc. Ab initio calculations on the silicate garnet pyrope have shown that *short-range* cation−cation repulsion is negligible.[30] Y^{3+} and the rare-earth trivalent ions were considered as unpolarizable species. van der Waals forces were neglected for all but the O^{2-}−O^{2-} interactions. The above approximations, even if they may represent severe simplifications, resulted in a consistent and well-optimized set of parameters. For the Al−O, Fe−O, and Ga−O *short-range* interactions the parameter A was allowed to take a different value depending on the site considered (octahedral or tetrahedral).[31] For the Fe−O interaction, the A parameter is virtually unaffected by the site, whereas for Al−O and Ga−O interactions only small variations are observed. The quality of the potentials was tested by calculation of lattice parameters, lattice properties, and mean thermal expansion coefficient in the range 25−800 °C. Because the cell parameter changes with temperature, calculation of the thermal expansion is a good test for the adopted potentials. The calculated properties were compared with experimental data[11,12,22,32] as well as with theoretical values obtained from ab initio electronic structure calculation.[25,33] As shown in Table 2, the agreement is generally rather good. The error on the unit cell edge is in most cases ≤0.1%. The static dielectric constant of $Y_3Fe_5O_{12}$ and $Gd_3Fe_5O_{12}$ was measured on high-density sintered pellets prepared at the Institute of Energetics and Interphases (IENI) of Genova.

Table 1. Interatomic Potential Parameters

(A) Short Range

interaction	cation radius (Å)	*A* (eV)	*ρ* (Å)
O^{2-}−O^{2-} [a]		22764.3	0.14900
Al^{3+}(a)−O^{2-}	0.56	1084.9	0.32346
Al^{3+}(d)−O^{2-}		1031.6	0.32346
Fe^{3+}(a,d)−O^{2-}	0.645	965.3	0.34240
Fe^{2+}−O^{2-} [b]	0.76	1207.6	0.30840
Ga^{3+}(a)−O^{2-}	0.62	1117.0	0.32977
Ga^{3+}(d)−O^{2-}		1102.2	0.32977
Y^{3+}−O^{2-}	1.015	1116.1	0.35451
Lu^{3+}−O^{2-}	0.97	1063.1	0.35187
Yb^{3+}−O^{2-}	0.98	1040.3	0.35424
Er^{3+}−O^{2-}	1.00	990.3	0.35978
Tb^{3+}−O^{2-}	1.045	893.5	0.37124
Gd^{3+}−O^{2-}	1.06	858.4	0.37568
Eu^{3+}−O^{2-}	1.07	804.9	0.38183
Sm^{3+}−O^{2-}	1.09	854.9	0.37910
Nd^{3+}−O^{2-}	1.12	781.3	0.38931
La^{3+}−O^{2-}	1.18	711.7	0.40580

(B) Shell Model

species	*Y* (e)	*k* (eV Å^{-2})
O^{2-}	−2.780	37.91
Al^{3+}	2.983	181.66
Fe^{3+}	5.612	188.18
Ga^{3+}	2.980	77.95
Fe^{2+}	2.997	62.9

[a] For the O^{2-}−O^{2-} interaction, *C* is 27.8 eV Å^6. [b] Lewis and Catlow, ref 31.

(2) Stability of Garnets. The stability of the garnets with respect to the parent binary oxides has been examined. The formation energy was estimated as the difference between the lattice energy of the garnet and the lattice energy of the parent oxides. Because the formation energy per formula unit of garnet is a small difference (of the order of −1 eV) between large numbers (the lattice energy of garnets is of the order of −600 eV), it is a quantity quite challenging to compute. Indeed, small variations of the interatomic potential parameters lead easily to variations of the lattice energy of this order of magnitude. Consequently, whereas the absolute value of the calculated formation energy is of little significance, the trends are more meaningful. The formation energy plotted against the Ln^{3+} ionic radius has a minimum for all three series of garnets and this suggests that the stability of the ternary compound is dominated by deviation of the ionic radius of the rare-earth from the optimum size. For solids, changes in internal energy are generally very similar to changes in enthalpy. The calculated formation energy compares

(29) Gale, J. D. *J. Chem. Soc., Faraday Trans.* **1997**, *93*, 629.
(30) D'Arco, Ph.; Freyria Fava, F.; Dovesi, R.; Saunders, V. R. *J. Phys.: Condens. Matter* **1996**, *8*, 8815.
(31) Lewis, G. V.; Catlow, C. R. A. *J. Phys C: Solid State Phys.* **1985**, *18*, 1149.
(32) Larsen, P. K.; Metselaar, R. *Phys. Rev. B* **1973**, *8*, 2016.
(33) Ching, W. Y.; Gu, Z.-Q.; Xu, Y.-N. *J. Appl. Phys.* **2001**, *89*, 6883.

Table 2. Crystal Structure and Properties of Selected Garnets: Experimental Values (in brackets) from References 11−12, 22, and 32

	$Y_3Al_5O_{12}$	$Y_3Fe_5O_{12}$	$Gd_3Fe_5O_{12}$	$Y_3Ga_5O_{12}$	$Gd_3Ga_5O_{12}$
cell edge (Å)	12.019 (*12.008*)	12.378 (*12.376*)	12.468 (12.470)	12.293 (12.280)	12.380 (12.377)
O position					
x_o	−0.0248 (*−0.0299*)	−0.0215(*−0.027*)	−0.0216 (*−0.0269*)	−0.0222(*−0.0272*)	−0.0222(*−0.0284*)
y_o	0.0524 (*0.0506*)	0.0544 (*0.0569*)	0.0521 (*0.0550*)	0.0542 (*0.0558*)	0.0518 (*0.0549*)
z_o	0.1513 (*0.1488*)	0.1524 (*0.1505*)	0.1524 (*0.1478*)	0.1519 (*0.1501*)	0.1518 (*0.1497*)
elastic constants (GPa)					
c_{11}	338.0 (*333.2*)	276.1 (*268.0*)	260.3 (*273.1*)	302.1 (*290.3*)	285.4 (*287.0*)
c_{12}	136.5 (*110.7*)	119.9 (*110.6*)	115.4 (*125.0*)	120.5 (*117.3*)	115.8 (*116.0*)
c_{44}	106.4 (*115.0*)	76.1 (*76.6*)	70.7 (*74.1*)	96.2 (*95.5*)	91.4 (*90.4*)
ϵ_0[a]	10.9 (*11*)	17.8 (*16.7,18,17*[d])	20.9 (*22*[d])	11.3	12.8 (*12.1*)
ϵ_∞[b]	3.5 (*3.5, 4.6*[c])	5.1 (*5.3, 5.5*[c])	5.1	3.4	3.4
TEC (K^{-1}) × 10^6 (25−800 °C)	6.5 (*8.5*)	12.5 (*10.6−11.9*)	12.2 (*10.3*)	7.7 (*9.2*)	8.7 (*9.0*)

[a] Static dielectric constant. [b] High-frequency dielectric constant. [c] From ab initio electronic structure calculations, refs 25 and 33. [d] Measured at the Institute of Energetics and Interphases on high-density sintered ceramics.

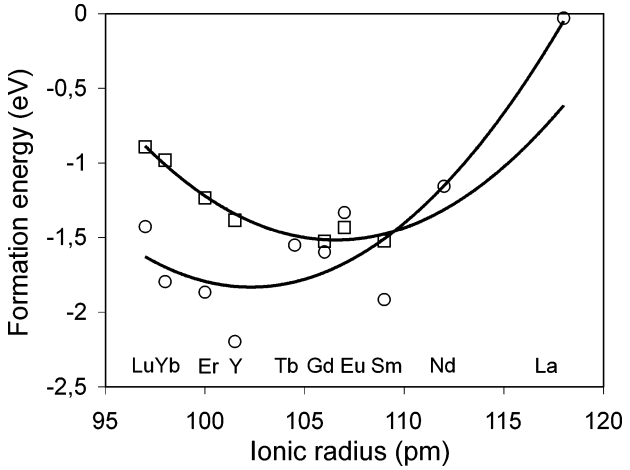

Figure 1. Calculated heat of formation (○) and experimental enthalpy (□) of formation of gallium garnets from the binary oxides. Solid lines correspond to the least-squares fit of data with a 2nd order polynomial.

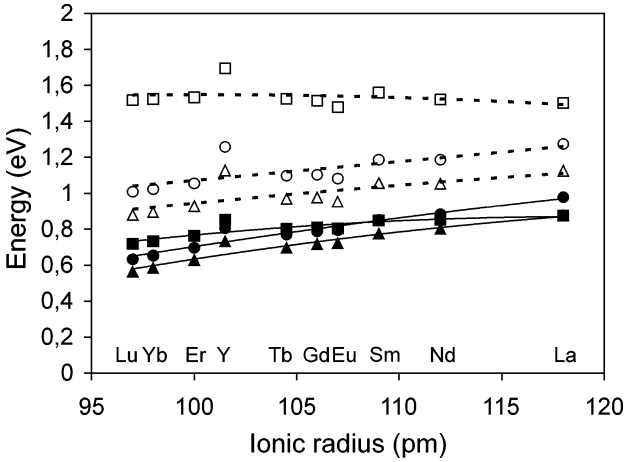

Figure 2. Energy of formation (per defect) of antisite cation pairs in $A_3B_5O_{12}$ (reaction 3): (□, ■) Al garnets; (○, ●) Ga garnets; (△,▲) Fe garnets. Full symbols correspond to A^{3+} antisite located at octahedral sites (a). Open symbols correspond to A^{3+} antisite located at tetrahedral sites (d). Lines correspond to the least-squares fit of data with a 2nd order polynomial.

favorably with the experimental values of the enthalpy of formation reported in a recent investigation on the thermodynamic stability of garnets,[34] as shown in Figure 1 for Ga garnets. Unfortunately, there are not experimental data available for $Nd_3Ga_5O_{12}$ to confirm the presence of a minimum. Nevertheless, the upward curvature of the enthalpy of formation is evident. A very similar behavior is predicted for $Ln_3Fe_5O_{12}$ garnets. In both cases, the formation energy increases rapidly for Ln = Nd, La. For Al garnets the minimum of the formation energy falls at the ionic radius of Er^{3+}. The calculated formation energy of $Nd_3Al_5O_{12}$ and $La_3Al_5O_{12}$ is positive. For all three series, the garnets of the largest rare-earths are predicted to be less stable than the garnets of smaller rare-earths. Experimentally, the compounds $Nd_3Fe_5O_{12}$, $La_3Fe_5O_{12}$, and $La_3Ga_5O_{12}$, as well the garnets $Ln_3Al_5O_{12}$ with Ln = Eu−La, are not observed, and they are replaced by the two-phase mixture $LnBO_3$ (perovskite) + B_2O_3 (corundum-type structure) in the A_2O_3−B_2O_3 phase diagrams (B = Al, Fe, Ga).[34] Nevertheless, the inclusion of these hypothetical compounds in the calculations has been useful to understand the trends involved in the defect formation energy in garnets.

(3) Cation Disorder. In garnets, the cation antisite is the lowest-energy intrinsic disorder mechanism, as already reported in previous studies on YAG and YIG.[21−23] The formation of an antisite pair involves the interchange of A^{3+} and B^{3+} ions on their lattice sites. Following the notation of Kroger and Vink,[35] this process can be represented as

$$A_A^\times + B_{B(s)}^\times \rightarrow A_{B(s)}^\times + B_A^\times \qquad (3)$$

where the subscript (*s*) denotes the lattice site of the B ion, either octahedral (a) or tetrahedral (d). The results are shown in Figure 2. The octahedral site is energetically favored with respect to the tetrahedral site. The energy change for reaction 3 (*s* = *a*) increases from 0.6−0.7 to 0.9−1.0 eV per defect increasing the ionic radius of the A^{3+} ion. Accordingly, formation of antisite pairs is easier for the small lanthanides, like Lu^{3+} and Yb^{3+}. The energy change for formation of antisite pairs involving the (d) site is ≈0.3 (Fe and Ga garnets) to 0.6−0.8 eV (Al garnets) higher. The trends reported in Figure 2 can be related to the variation of the ionic radius of A^{3+} and B^{3+}. For sake of comparison, the formation energy of Schottky-like defects ranges from 2.4 to 5 eV per defect depending on the garnet and on the defect

(34) Kanke, Y.; Navrotsky, A. *J. Solid State Chem.* **1998**, *141*, 424.

(35) Kröger, F. A. *The Chemistry of Imperfect Crystals*; North-Holland: Amsterdam, 1964.

reaction considered. For Frenkel-like defects, the formation energy is even higher.

(4) Nonstoichiometry. The main objective of this study is to investigate the mechanisms responsible for nonstoichiometry in garnets and then correlate the results with the homogeneity range of these compounds and the behavior experimentally observed. The investigation was restricted to the defect reactions leading to nonstoichiometric, single-phase compounds. Defect reactions where nonstoichiometry is accompanied by the formation of a secondary phase correspond to two-phase regions of the phase diagrams. Furthermore, only the defect reactions corresponding to the lowest energy changes were thoroughly investigated. Besides the accommodation of deviation from stoichiometry by formation of antisite defects alone, also reactions involving the formation of cation and oxygen vacancies were considered. Namely:

A_2O_3 excess (A = Y, Lu−La)

$$4A_2O_3 + 5B^{\times}_{B(s)} \rightarrow 5A^{\times}_{B(s)} + A_3B_5O_{12} \quad (4)$$

$$3A_2O_3 + 5B^{\times}_{B(s)} + 3O^{\times}_{O} \rightarrow 3A^{\times}_{B(s)} + 2V'''_{B(s)} + 3V^{\bullet\bullet}_{O} + A_3B_5O_{12} \quad (5)$$

B_2O_3 excess (B = Al, Ga, Fe)

$$4B_2O_3 + 3A^{\times}_{A} \rightarrow 3B^{\times}_{A} + A_3B_5O_{12} \quad (6)$$

$$3B_2O_3 + 3A^{\times}_{A} + 3O^{\times}_{O} \rightarrow B^{\times}_{A} + 2V'''_{A} + 3V^{\bullet\bullet}_{O} + A_3B_5O_{12} \quad (7)$$

In the case of iron garnets, formation of oxygen vacancies and related oxygen nonstoichiometry can occur as a consequence of reduction of a fraction of Fe(III) to Fe(II). Two mechanisms were considered:

$$6Fe^{\times}_{Fe(s)} + 3O^{\times}_{O} \rightarrow \frac{3}{2}O_2(g) + 3V^{\bullet\bullet}_{O} + 6Fe'_{Fe(s)} \quad (8)$$

$$6Fe^{\times}_{Fe(s)} + 3O^{\times}_{O} + 6A^{\times}_{A} \rightarrow \frac{3}{2}O_2(g) + 3V^{\bullet\bullet}_{O} + 6Fe'_{A} + 6A_{Fe(s)} \quad (9)$$

where $Fe'_{Fe(s)}$ and Fe'_{A} denote an Fe^{2+} ion on a regular iron site and on an A site, respectively. Oxygen vacancies and antisite defects are both included in reaction 9. The defect energy resulting from calculations was combined with other relevant energetic terms, like calculated lattice energy of binary oxides and garnets (reactions 4−7), third ionization potential of iron, dissociation energy of oxygen molecule, and the sum of the first and second affinities of oxygen (reactions 8−9) to obtain the energy change of the above reactions.[13] In the following, the energy change is always referred to 1 mole of excess A or B (reactions 4−7) or to 1 mole of divalent iron (reactions 8−9). The energy change is always referred to isolated, noninteracting defects (infinite dilution). The interaction between oppositely charged defects is discussed in the next section in the case of oxygen vacancies.

Figure 3 shows the results for the solution of excess A_2O_3 by reaction 4. It is evident that incorporation of the lanthanide ion on the octahedral (a) site is favored

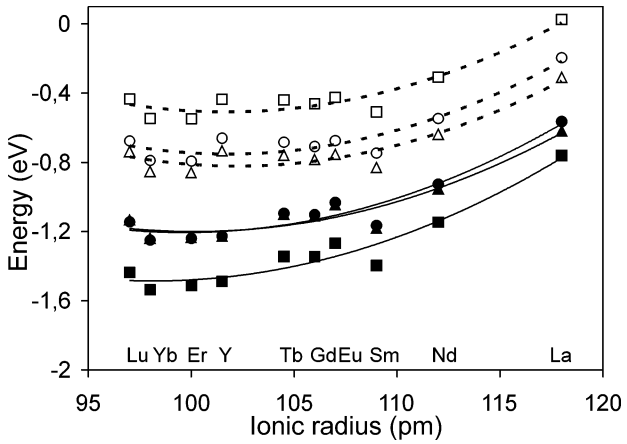

Figure 3. Energy of solution (per A atom) of excess A_2O_3 in $A_3B_5O_{12}$ (reaction 4): (□, ■) Al garnets; (○, ●) Ga garnets; (△,▲) Fe garnets. Full symbols refer to incorporation of A^{3+} at the octahedral site. Open symbols refer to incorporation of A^{3+} at the tetrahedral site. Lines correspond to least-squares fit of data with a 2nd order polynomial.

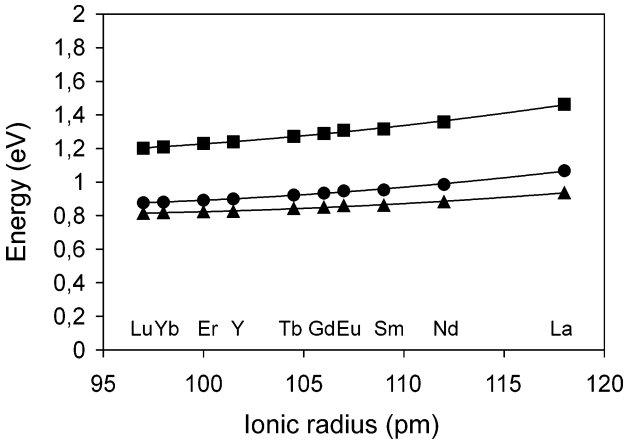

Figure 4. Energy of solution (per B atom) of excess B_2O_3 in $A_3B_5O_{12}$ (reaction 6); (■) Al garnets; (●) Ga garnets; (▲) Fe garnets. Solid lines correspond to least-squares fit of data with a 2nd order polynomial.

in comparison to incorporation on the tetrahedral (d) site. In any case, the energy change of reaction 4 is negative and strongly dependent on the ionic radius of A^{3+}. For Fe and Ga garnets, the solution energy of the rare-earth oxide ranges from −1.2 to −0.6 eV. For Al garnets, the reaction is 0.2−0.3 eV more exothermic. The results also suggest that the solution energy reaches a plateau or even a minimum for $A^{3+} = Er^{3+}/Y^{3+}$.

When incorporation of excess B_2O_3 (B = Al, Fe, Ga) by reaction 6 is considered (Figure 4), the solution energy is 2−2.5 eV higher than the incorporation of excess A_2O_3 by reaction 4 (octahedral site). Therefore, it can be predicted that nonstoichiometry in garnets will be predominantly associated with the incorporation of an excess of Y_2O_3 or Ln_2O_3. This result is somewhat different from that reported in previous simulation studies[21−23] where the energy change associated with reactions 4 and 6 resulted to be similar within 0.5 eV. The predicted strong asymmetry of the deviation from stoichiometry is well confirmed by the experimental data in the case of Ga garnets. Schneider et al.[36] carried out an extensive study on the phase diagrams of garnet-

forming systems. They found that the solubility of excess yttrium or rare-earth oxide rapidly increases (≈1 at. % for Sm, ≈12 at. % for Er) with decreasing rare earth radius until Tm^{3+} (intermediate between Er^{3+} and Yb^{3+}) is reached, then slightly decreases (≈11% for Lu). Later investigations have confirmed these earlier results.[37−39] In contrast, solubility of excess Ga_2O_3 is reported to be very small or negligible.[36−39] Therefore, there is a clear, although qualitative, correlation between the energy change of reaction 4 and the solubility of excess Y_2O_3 or Ln_2O_3 in gallium garnets.

In the case of Al garnets, the incorporation of an appreciable excess (2−3 at. %) of the rare-earth oxide was detected only for $Lu_3Al_5O_{12}$ and $Yb_3Al_5O_{12}$.[36] Solution of excess Y_2O_3 in $Y_3Al_5O_{12}$ originally reported by Keith and Roy[40] has not been confirmed in later studies, and YAG is usually described as a stoichiometric compound.[41,42] Iron garnets were reported as stoichiometric compounds by Schneider et al.[36] Only the Y_2O_3−Fe_2O_3 and Gd_2O_3−Fe_2O_3 phase diagrams were carefully reinvestigated.[43−46] In both cases, deviation of the A/B ratio from 3/5 is reported to be very small. Even considering that deviations from stoichiometry ≤ 1 at. % are difficult to detect experimentally and the lack of data for several systems, the results of our calculations (Figure 3) do not account for the different behavior of Al and Fe garnets with respect to Ga garnets. However, Schneider et al.[36] observed that garnet solid solution occurred only in systems in which the perovskite-type compound ABO_3 does not exist as a stable phase. Very likely, the incorporation of excess Y_2O_3 or Ln_2O_3 in the garnet phase is in competition with the formation of the two-phase mixture $ABO_3 + A_3B_5O_{12}$ by reaction

$$A_3B_5O_{12} + A_2O_3 \rightarrow 5ABO_3 \qquad (10)$$

When the perovkite phase is stable, formation of the two-phase mixture is probably preferred. The foregoing interpretation was corroborated by the calculation of the energy of solution of excess A_2O_3 by the reaction

$$A_2O_3 + B^{\times}_{B(s)} \rightarrow A^{\times}_{B(s)} + ABO_3 \qquad (11)$$

where formation of the perovskite phase is taken into account. The lattice energy of orthorhombic perovskites was obtained using the garnet potential parameters. The resulting solution energies (per A atom) are comparable, within 0.1−0.3 eV to the values obtained for reaction 4 (Figure 3). The data obtained by Kuklja[23] in the case of $Y_3Al_5O_{12}$ led to the same conclusion. However, it should be stressed that a meaningful comparison between reactions 4 and 11 would require for the perovskites a set of fully optimized potential parameters following the same approach as that adopted for garnets. This is not an easy task, because the lattice properties of most perovskites involved in reaction 11 are unknown and the fitting would be forced to reproduce only the crystal structure rather than the whole set of properties. In any case, atomistic simulation is generally unable to provide a reliable conclusion when processes whose energy differs only for some tenths of eV are compared because of the approximations and limitations inherent to the technique.

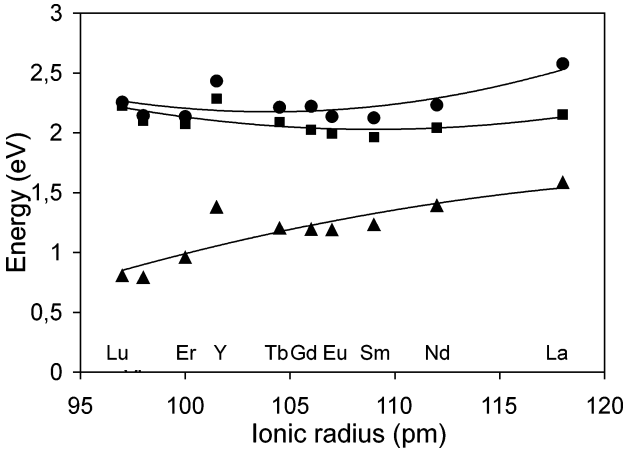

Figure 5. Energy of solution (per A atom) of excess A_2O_3 in $A_3B_5O_{12}$ (reaction 5). A^{3+} is incorporated at the octahedral site: (■) Al garnets; (●) Ga garnets; (▲) Fe garnets. Lines correspond to least-squares fit of data with a 2nd order polynomial.

Accommodation of nonstoichiometry by simultaneous formation of antisite defects, cation vacancies, and oxygen vacancies (reactions 5 and 7) is considerably less favorable than formation of antisite defects (reactions 4 and 6) alone. In turn, reaction 7 is energetically less favorable than reaction 5 by 1−2 eV. Figure 5 shows the energy for solution of excess A_2O_3 assuming incorporation of the rare-earth ion at the octahedral site (lower energy). For Al and Ga garnets, the solution energy is 2−2.5 eV per rare earth atom. Consequently, the concentration of intrinsic vacancies is predicted to be rather low. Excess of neither A_2O_3 or B_2O_3 appears to be a major source of oxygen vacancies in Al and Ga garnets. This result supports the defect models developed for these compounds on the basis of electrical conductivity measurements. According to these models, formation of oxygen vacancies is dominated by the presence of accidental or intentional acceptor impurities while the contribution of intrinsic vacancies is usually negligible.[5−7,9−10] For iron garnets, the energy change associated with reaction 5 (octahedral site) is lower (1−1.5 eV) and decreases with decreasing A^{3+} cation size. Therefore, formation of intrinsic vacancies in iron garnets, in particular for the compounds of the smaller rare earth elements, seems easier in comparison to that of other garnets.

However, the preferred mechanisms to accommodate oxygen nonstoichiometry in iron garnets are represented by reactions 8 and 9, as shown in Figure 6. Divalent iron ions created by reduction of Fe(III) behave as intrinsic acceptors, and their negative charge is com-

(36) Schneider, S. J.; Roth, R. S.; Waring, J. L. *J. Res. Nat. Bur. Stand.* **1961**, *65A*, 345.
(37) Geller, S. *Z. Kristallogr.* **1967**, *125*, 1.
(38) Allibert, M.; Chatillon, C.; Mareschal, J.; Lissalde, F. *J. Cryst. Growth* **1974**, *23*, 289.
(39) Nicolas, J.; Coutures, J.; Coutures, J. P.; Boudot, B. *J. Solid State Chem.* **1984**, *52*, 101.
(40) Keith, M. L.; Roy, R. *Am. Mineral.* **1954**, *39*, 1.
(41) *Phase Diagrams for Ceramists*, Vols. I−XII; The American Ceramic Society: Westerville, OH, 1969−2000.
(42) Fabrichnaya, O.; Seifert, H. J.; Ludwig, T.; Aldinger, F.; Navrotsky, A. *Scand. J. Metall.* **2001**, *30*, 175.
(43) Van Hook, H. J. *J. Am. Ceram. Soc.* **1961**, *44*, 208.
(44) Van Hook, H. J. *J. Am. Ceram. Soc.* **1962**, *45*, 162.
(45) Paladino, A. E.; Maguire, E. A. *J. Am. Ceram. Soc.* **1970**, *53*, 98.
(46) Van Hook, H. J. Phase Equilibria in Magnetic Oxide Materials. In *Phase Diagrams - Materials Science and Technology*; Academic Press: San Diego, CA, 1976; Vol IV, pp 193−232.

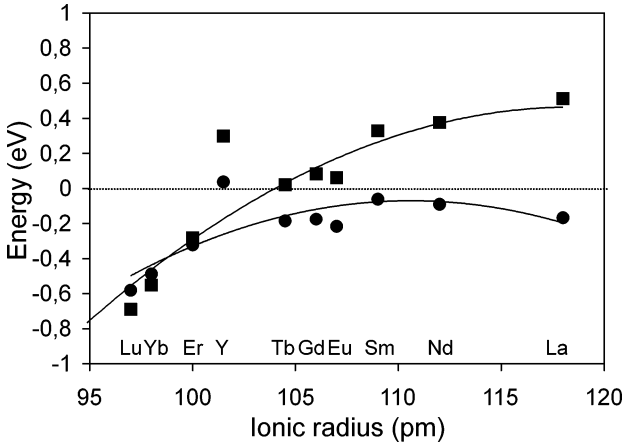

Figure 6. Energy for accommodation of oxygen nonstoichiometry in $A_3Fe_5O_{12}$ (per divalent Fe ion): (●) Reaction 8 (Fe^{2+} located at octahedral site); (■) Reaction 9 (A^{3+} antisite located at octahedral site). Lines correspond to least-squares fit of data with a 2nd order polynomial.

pensated by creation of oxygen vacancies. Accommodation of oxygen nonstoichiometry by reaction 8 is rather favorable, with the energy change being in the range −0.6 to 0 eV. This result agrees with the observation that $Y_3Fe_5O_{12}$ can be easily reduced at high temperature, even in air.[43−45] The existence of an energetically favorable mechanism for formation of oxygen vacancies in iron garnets also explains the much higher oxygen conductivity of $Gd_3Fe_5O_{12}$ in comparison to that of $Gd_3Ga_5O_{12}$ and $Y_3Al_5O_{12}$.[7,8] The data reported in Figure 6 correspond to Fe^{2+} located at the octahedral site; however, the energy values are practically unchanged for substitution at the tetrahedral site. Reaction 8 has been proposed to be the main process responsible for deviation from stoichiometry in $Y_3Fe_5O_{12}$ at high temperature or at low oxygen pressure.[9,10] Our results strongly indicate that the same mechanism can be extended to all iron garnets. If a small polaron model is assumed to describe the transport of electronic carriers in garnets, the divalent iron ions are equivalent to electrons localized on regular Fe^{3+} ions.[9,10,21] Consequently, reaction 8 also accounts for n-type conduction in iron garnets. Formation of antisite pairs $Fe'_A - A_{Fe(a)}$ (reaction 9) is less favorable (by 0.4−0.6 eV) for the larger rare earth ions, whereas it is energetically comparable to reaction 8 for the smaller rare earth elements. If the lanthanide ion is located at the tetrahedral site, the energy increases by 0.5−0.6 eV. In any case it is predicted that reduction and formation of oxygen vacancies are significantly easier for $Lu_3Fe_5O_{12}$, $Yb_3Fe_5O_{12}$, and $Er_3Fe_5O_{12}$ in comparison to other iron garnets. The tendency to reduction of iron garnets suggests also a simple way to control electrical conductivity and concentration of oxygen vacancies in Al and Ga garnets by formation of solid solutions with Fe garnets. This method would overcome the small solubility and the tendency to segregation exhibited by many dopants. The feasibility of this approach has been shown by Rotman and Tuller[7] in the case of $Y_3Al_5O_{12}$ containing different concentrations of $Y_3Fe_5O_{12}$ in solid solution.

The possible coexistence of oxygen nonstoichiometry, substitutional divalent iron, and deviation of the A/Fe ratio from 3/5 in iron garnets has been also investigated. For the reaction

$$4Fe_2O_3 + 3O_O^{\times} + 3A_A^x + 5Fe_{Fe(a)}^x \rightarrow 2Fe_A^{\times} + 5Fe'_{Fe(a)} + Fe'_A + 3V_O^{\bullet\bullet} + \frac{3}{2}O_2(g) + A_3Fe_5O_{12} \quad (12)$$

an energy change of 8 to 9 eV per divalent iron can be calculated. This value is prohibitively high and the above reaction is not predicted to take place.

(5) Divalent Iron − Oxygen Vacancy Clusters. It is well established that for some oxides, such as cubic ZrO_2[47] and some perovskites,[48,49] the oxygen ionic conductivity is limited by the extent of the interaction between the oxygen vacancy and the charge compensating defect, usually a dopant ion. At low defect concentration a simple description of these interactions is the formation of defect pairs. The magnitude of the interaction can be described by the binding energy of the cluster, i.e., the difference between the sum of the formation energies of the isolated defects and the formation energy of the defect pair. Therefore, a positive binding energy denotes a stable cluster. The greater the binding energy and the lower the temperature, the lower the fraction of isolated vacancies available for oxygen migration.

We have considered the formation of pair clusters in iron garnets comprised of divalent iron located at substitutional position (a, c, and d sites) and an oxygen vacancy in its first coordination sphere: $(Fe'_{Fe(s)}:V_O^{\bullet\bullet})^{\bullet}$ and $(Fe'_A:V_O^{\bullet\bullet})^{\bullet}$. When Fe^{2+} is located at the octahedral site (Figure 7), the binding energy increases from ≈−0.1 up to ≈0.5 eV moving from Lu to Tb garnet, then slightly decreases for larger rare earths. For the lutetium garnet there is no tendency to clustering, at least at relatively low defect concentration. However, at higher defect concentration other types of clusters could have greater stability. For ytterbium and erbium garnets the binding energy is positive (0.2−0.3 eV), but lower than that of the garnets of the larger rare earths. This means that even at moderately high temperatures (300−400 °C), the majority of the oxygen vacancies will not be bound in clusters. When the Fe^{2+} ion is located at tetrahedral (d) site, the binding energy gradually increases from ≈0.2 to 0.5 eV with increasing the A^{3+} cation size. For substitution of Fe^{2+} at the dodecahedral (c) site, the binding energy exhibits a behavior similar to that found for substitution at the octahedral site, with a maximum value of ≈0.7 eV for Tb garnet. Again, clusters formed in Lu and Yb garnets are less stable, with the binding energy being of the order of 0.1−0.2 eV.

IV. Summary and Conclusions

Disorder and nonstoichiometry in synthetic garnets $A_3B_5O_{12}$ have been systematically investigated as a function of the ionic radius of A^{3+} (A = Y, Lu−La) and B^{3+} (B = Al, Ga, Fe). Only the energetically most favored mechanisms have been considered, and calculations have been restricted to defect reactions leading to

(47) Zacate, M. O.; Minervini, L.; Bradfield, D. J.; Grimes, R. W.; Sickafus, K. E. *Solid State Ionics* **2000**, *128*, 243.
(48) Khan, M. S.; Islam, M. S.; Bates, D. R. *J. Phys. Chem. B* **1998**, *102*, 3099.
(49) Merkle, R.; Maier, J. *Phys. Chem. Chem. Phys.* **2003**, *5*, 2297.

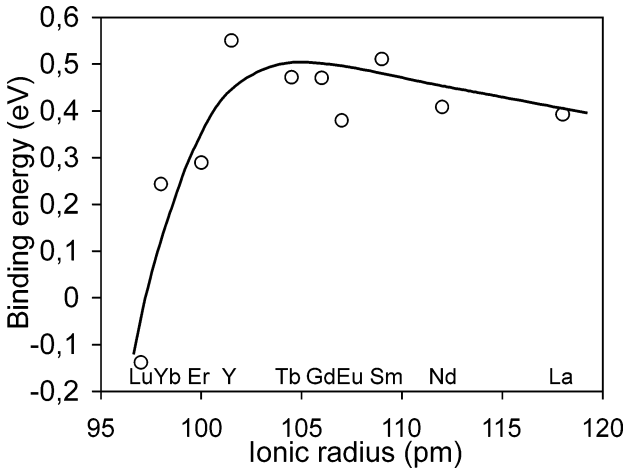

Figure 7. Binding energy of Fe^{2+} to a nearest neighbor oxygen vacancy in $A_3Fe_5O_{12}$. The Fe^{2+} ion is located at the octahedral (*a*) site. The line is a guide for the eyes.

single-phase garnets. Given the limitations of the static-lattice technique adopted in this work, we have focused on trends rather than on the absolute reaction energies. The inclusion of some hypothetical garnet compounds has allowed investigation of the trends over a broader range of the A cation radius.

The following general conclusions can be drawn. (1) Disorder in garnets is associated with the formation of antisite cation defects. Formation of Schottky and Frenkel disorder involves much higher energies. The energy of disorder decreases with decreasing the A^{3+} ionic radius. Substitution of A^{3+} at the octahedral site is favored with respect to substitution at tetrahedral site. (2) Incorporation of excess Y_2O_3 or rare earth oxide in the garnet phase is energetically preferred in comparison to incorporation of excess B_2O_3 (B = Al, Fe, Ga). This result explains the strong asymmetry experimentally found for nonstoichiometry in garnets. The trend of the solution energy is in qualitative agreement with the available solubility data of A_2O_3 in gallium garnets. For Al and Fe garnets, incorporation of excess A_2O_3 is in competition with formation of the two-phase $A_3B_5O_{12}$–ABO_3 mixture. However, owing to the limitations of the present calculations, it is not possible to define the most probable process. (3) Excess of neither A_2O_3 or B_2O_3 appears to be the main source of oxygen vacancies in Al and Ga garnets. Consequently, the concentration of intrinsic oxygen vacancies is predicted to be rather small in these compounds, and oxygen ionic conductivity will be mainly associated with intentional or accidental doping. (4) An energetically favored mechanism for oxygen nonstoichiometry in Fe garnets is provided by the easy reduction of Fe^{3+} to Fe^{2+}. The resulting excess of negative charge is compensated by formation of oxygen vacancies. The energy for formation of oxygen vacancies decreases with decreasing A^{3+} ionic radius. Consequently, Lu, Yb, and Er iron garnets can be regarded as the most promising compounds of the garnet family for potential applications as oxygen conductors at high temperature. With increasing defect concentration, formation of $(Fe':V_O^{\bullet\bullet})^{\bullet}$ defect pairs in iron garnets becomes possible. However, the binding energy is lower for the garnets of the smaller rare earths.

The calculated trends provide useful suggestions for future experimental studies. Furthermore, the trends can be used predictively for rare-earth elements that have not been explicitly included in the modeling.

Acknowledgment. We thank Dr. M. Viviani for the measurement of the dielectric constant of some of the investigated garnets and Dr. P. Baldini for his computing technical support.

CM031138U